




## Photocatalytic efficiency test stand

Dominik Novotný<sup>1</sup>, Tibor Dzuro<sup>1\*</sup>, Ján Král<sup>1</sup>, Jakub Hajtol<sup>2</sup>

<sup>1</sup> Department of Production Systems and Robotics, Faculty of Mechanical Engineering, Technical University of Košice, Letná 1/9, Košice, Slovak Republic

<sup>2</sup> Department of Logistics and Transport, Faculty of Mining, Ecology, Process Control and Geotechnologies, Technical University of Košice, Letná 1/9, Košice, Slovak Republic

\* Corresponding author's e-mail: [tibor.dzuro@tuke.sk](mailto:tibor.dzuro@tuke.sk)

### ABSTRACT

This paper details the development and characterization of a photocatalytic efficacy test stand that was designed in response to an urgent global requirement for efficient and economically viable methods of pathogen elimination, such as the COVID-19 pandemic. The primary objective was to establish a robust methodology for evaluating the performance of a new type of device integrating an innovative photocatalytic antimicrobial core. This core is based on a specially engineered polypropylene fabric, active under normal illumination, which generates reactive oxygen species (ROS) for the destruction of pathogens, including viral agents. The design of the test stand was precisely engineered in SolidWorks and is protected by a utility model. The stand allows quantitative assessment of photocatalytic degradation by monitoring the concentration of toluene as a model volatile organic compound via a mass spectrometer. This system verifies the significant oxidation capacity and broad-spectrum potential of the test material for effective decontamination of the air environment. The developed test stand represents a versatile tool for further research and optimization of photocatalytic materials and is suitable for testing efficacy against both organic and inorganic compounds. It thus contributes to a major improvement in the quality of the indoor environment and the protection of public health.

**Keywords:** test stand, photocatalysis, antimicrobial core, polypropylene fabric, methodology

### INTRODUCTION

In recent decades, air quality and the spread of pathogens have become one of the most pressing global challenges [1, 4, 9, 12]. Population growth, urbanization, and industrial activity have led to significant air pollution that has demonstrable negative impacts on human health and ecosystems [47, 52]. In addition to chemical pollutants, biological agents such as bacteria, viruses, and fungal spores, which may spread through the air and cause infectious diseases, pose a serious threat [2, 3, 7, 8, 11, 13]. The recent COVID-19 pandemic has particularly highlighted the critical need for efficient, safe, and cost-effective technologies to decontaminate indoor environments [5, 6, 10].

Traditional methods of air purification, including mechanical filtration [20, 24], UV

germicidal irradiation [14, 21, 17], chemical disinfection [14, 15, 23], or the use of ozone [27, 29], often have limitations. Air ionization, although offering alternative approaches to purification [18], also has its specificities in the context of human health impact [19]. These may include high energy intensity [16], formation of harmful by-products [22, 28], limited effectiveness against a wide range of contaminants [23, 15], or requirements for specific operating conditions and maintenance [25]. Although advanced approaches have been developed [25, 26], there is still room for innovative and sustainable solutions to overcome these barriers [30–33].

In this context, photocatalysis has established itself as a particularly promising environmental technology [34–36]. It is a chemical process in which a photocatalyst, activated by light energy,

catalyzes oxidation and reduction reactions [34, 42]. This process efficiently generates highly reactive oxygen species (ROS) that can degrade a wide range of organic pollutants, including volatile organic compounds (VOCs) and pathogens [35, 37, 38]. An important advance is the development of photocatalysts capable of activity under conventional lighting, which increases their practical applicability and energy efficiency in indoor applications [39–41, 48].

The development and evaluation of new photocatalytic materials and systems require robust and reliable testing methodologies [42, 43]. Despite the existence of international ISO standards [44, 45] for the evaluation of photocatalytic activity, challenges remain, particularly regarding testing innovative nanomaterials [45] and direct verification of efficacy against biological agents under realistic conditions [5, 46]. Current evaluation methods are constantly evolving, including approaches to rapid, high throughput testing of photocatalytic activity [45]. There is often a lack of certified facilities for such specific testing, which necessitates the development of custom, adaptable test facilities [44].

This paper focuses on the detailed design, construction, and operational methodology of a custom photocatalytic efficiency test bench. The bench was precisely designed using computer-aided design (CAD) software [49, 51] and its design is protected by a utility model [50]. It is specifically designed to evaluate the performance of a new type of device that incorporates an innovative photocatalytic antimicrobial core. Monitoring of model substances such as toluene, whose physicochemical properties are well documented [53, 54], using an advanced mass spectrometer [52] is used to quantify performance. The aim of this work is to present a versatile and reliable tool for the comprehensive evaluation of photocatalytic materials, including their efficacy against both organic and inorganic compounds, thus contributing to the advancement of sustainable air purification and the protection of public health.

## PHOTOCATALYTIC PERFORMANCE TEST BENCH

Based on an analysis of the theoretical principles of photocatalysis and existing test procedures, including international ISO standards and innovative rapid methods, a specific approach

for the evaluation of the developed photocatalyst was designed and implemented. Due to the absence of certified workplaces in Slovakia for direct testing of antimicrobial filters with pathogens and the impossibility to work with such biological agents, it was necessary to develop a custom test bench for the assessment of photocatalytic efficacy. The aim was to verify the efficacy of the antimicrobial filter included in our test bench. [44–46]

In assessing our antimicrobial filter, which is based on a knitted fabric substrate and exhibits its activity in visible light (in the green to blue wavelength range), its effectiveness was tested using a model test substance, toluene. It was hypothesised that if the ability to eliminate the test substance (toluene) to the desired level was demonstrated, this would also confirm the ability to eliminate a variety of pathogens, including COVID-19 virus, for which the test stand was designed as a priority. A mass spectrometer is used to obtain realistic results of the performance of this test bench (Figure 1). This instrument is specialized to measure the concentration of a calibrated gas in space [52]. It is important to note that the mass spectrometer, although highly accurate, is not designed to simultaneously measure the concentration of multiple gases.

Calibration of the device is necessary before each measurement. To determine the efficiency of the polypropylene braid under test in the photocatalytic efficiency test device, the mass spectrometer will measure the concentration of the test gas before it enters the filter section and after it leaves the filter section [52]. The output of the device is data in electronic form, presented as a graph. In this way, it is demonstrated whether the test knitted fabric contained in the test device meets the required parameters or achieves the percentage efficiency. If the test knitted fabric eliminates the test gas, toluene, to 70% or more, it is assumed that the test fabric will also effectively eliminate any pathogens that will be present in the area.

The comprehensive methodology for evaluating photocatalytic efficacy is implemented using a specifically designed photocatalytic efficiency test stand. The operational principle of this stand is based on a continuous flow system designed to provide a controlled and reproducible environment for the photocatalytic degradation process. A high-level representation of the system's functional blocks is provided on Figure 2.



**Figure 1.** Mass spectrometer

As depicted in Figure 2, the test stand integrates several key functional components that work in synergy. The heating pad, for instance, is responsible for heating the test substance, specifically the toluene in the toluene dish. This precise temperature control, managed by the computer, ensures a consistent and stable input concentration of toluene-saturated air into the system.

Furthermore, the mixing device – propeller, coupled with the fan, is crucial for the suction of toluene-saturated air and for creating a homogeneous mixture. The speed control of this device, managed by the computer, ensures optimal dispersion of the toluene in the air stream, a critical factor for consistent interaction with the photocatalyst.

The core of the test stand is represented by the antimicrobial core, with both an inlet and an outlet, where the photocatalytic process occurs. A controllable light source provides the necessary illumination (within the 400–570 nm wavelength range as described later) to activate the photocatalyst. The design of this chamber maximizes the photocatalyst's surface area exposure to the contaminated air, leading to the production of purified air.

To quantify the degradation efficiency, a mass spectrometer is utilized as the input and output measurement system. This instrument takes

readings at the inlet measurement point (before the antimicrobial core) and the output measurement point (after the antimicrobial core). The collected data are then presented as a measurement graph, allowing for real-time monitoring of the degradation dynamics.

The computer serves as the central control and data acquisition unit for the entire system. It manages the temperature control for the heating pad and the speed control for the fan. Additionally, it processes the data from the mass spectrometer to generate the measurement graph and oversee overall system monitoring. This comprehensive control system allows for precise adjustment and monitoring of various experimental parameters, including illumination intensity, airflow rate, temperature, humidity, and even dust or general air pollution levels.

The experimental process begins by generating a stable, known concentration of toluene vapor, which is then thoroughly mixed with the air stream. This homogeneous mixture is subsequently directed through the antimicrobial core, where the light-activated photocatalyst initiates the degradation of toluene. The mass spectrometer continuously monitors the reduction in toluene concentration, providing real-time data on the photocatalytic efficiency. This robust setup ensures highly accurate and reproducible experimental conditions for the evaluation of new photocatalytic materials.

The test rig (Figure 3, Figure 4) itself, which is characterized by a transparent polymer tube (1), integrates a test substance generator with thermoregulation to control the evaporation rate (4), a suction and mixing system (5) and the antimicrobial core itself. This core consists of a knitted metal oxide polymer fibre and is supplemented by a controllable light source which is located on a central tube (3). For visual inspection of the process and access to the measurement probes, special holes are provided in the tube (2, 7). Air circulation in the bench is provided by a fan (5) and a mixing device in the form of a propeller (7) is used for optimised dispersion in the pre-filtration zone (6).

The efficiency of the antimicrobial filter is systematically monitored at two key locations: before entering the antimicrobial core and after leaving it, using a mass spectrometer. During experimental testing, the temperature can be flexibly controlled to optimize the evaporation rate, and the level of dust or general air pollution can

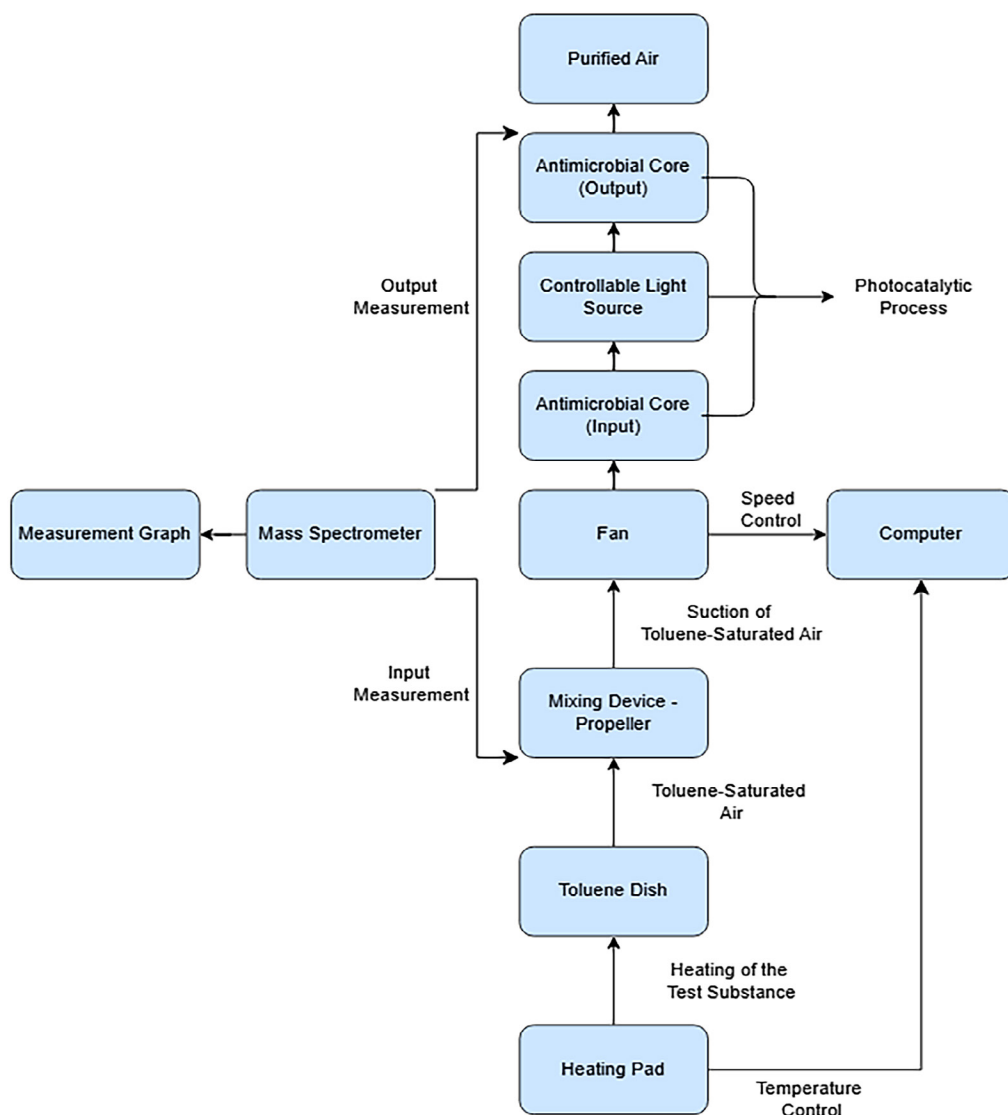


**Figure 2.** Block diagram of the photocatalytic test stand

also be monitored and modified. The versatility of the device allows the configuration of several operating parameters such as air flow volume per minute, temperature, humidity and dust level.

The main advantages of this technical solution include its adaptability for testing a variety of photocatalytic agents and their cleaning efficiency, with a proven broad spectrum effect on both organic and inorganic substances. Thanks to the integration of a mass spectrometer, the results can be evaluated instantaneously, with the possibility of continuously controlling the volume of air supplied to the core of the test rig. In addition to the basic experimental function, which is crucial for testing a wide range of compounds and optimizing the photocatalytic core, the test bench also allows for thorough material lifetime tests under controlled conditions, whereby a knitted

polymer fibre with metal oxides is applied. This comprehensive methodology, supported by a specifically designed test rig, allows not only to quantify the performance of our photocatalyst in an exact manner, but also to understand in detail its basic mechanisms of operation and to confirm its potential for large-scale practical applications in the field of indoor air decontamination.

## RESEARCH AND DEVELOPMENT OF A POLYPROPYLENE FIBRE PHOTOCATALYST

The current global challenges associated with pathogen elimination and environmental decontamination urgently require the development of



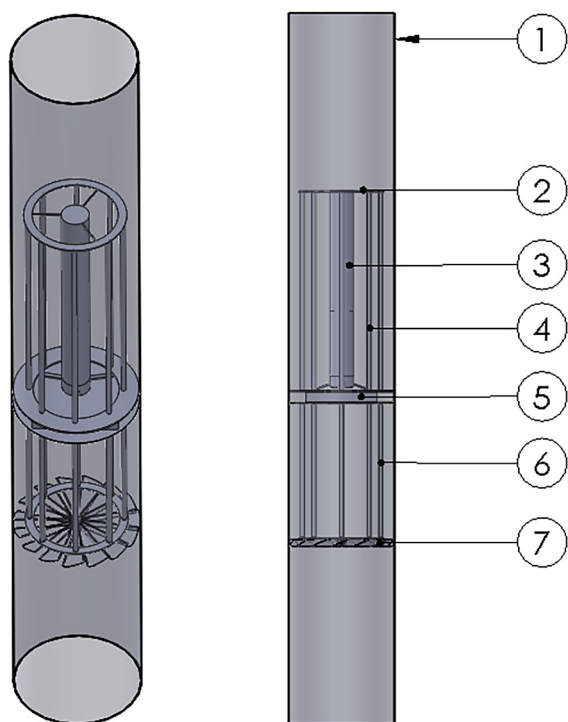


**Figure 3.** Photocatalytic efficiency test bench

innovative, energy-efficient and widely applicable solutions. This research presents a breakthrough concept of a photocatalyst with polypropylene braid as an essential component (Figure 5). This unique knitted fabric has been specially developed and is based on polypropylene fibres that are enriched with additives.

On the basis of proper knitted fabric selection, six knitted fabrics with different parameters were selected for testing. The knits fabric tested are detailed in Table 1, where their characteristics such as designation, fibre type, unit fineness, colour, knitting tension and areal density are included.

On the basis of these tests, the most suitable PL-3 knitted fabric was selected, characterised by a fibre fineness of 168 dTex and an areal density in the range 230–231 g/m<sup>2</sup>. This knit effectively absorbs radiation in the wavelength range 400–570 nm. On the basis of these aspects, PL-3 knitted fabrics exhibit exceptional antimicrobial activity already after exposure to the visible light spectrum, namely in the green to blue region, which corresponds to normal daytime illumination.

To calculate the required radiation power, the calculation for the mean wavelength required to activate the total amount of photocatalyst contained in 1 m<sup>2</sup> of fabric shows a requirement of 833 J of energy. This calculated energy can convert 0.43 mg of oxygen (O<sub>2</sub>) into a highly reactive



**Figure 4.** Photocatalytic efficiency test stand

form (corresponding to approximately  $1.6 \times 10^{19}$  molecules). At a dye and oxygen content of 25%, the maximum power that 1 m<sup>2</sup> of fabric will need to achieve maximum PL-3 knitting activity is approximately 16 W in the 400–570 nm radiation spectral range. For a broader radiation spectrum, approximately 3 W needs to be added for a total power of 19 W.

The graph in Figure 6 presents the spectral distribution of the radiation of a specific light source. The X-axis ( $\lambda$  (nm)) shows the wavelength of light in nanometers, while the Y-axis ( $\mu\text{W}/\text{cm}^2/\text{nm}$ ) indicates the radiation intensity in microwatts per square centimeter per nanometer. Visual interpretation of the graph shows that the measured spectrum extends from approximately 200 nm to 850 nm. Within this range, several emission peaks are clearly observable. A distinct peak is located around 435 nm, which corresponds to the blue component of the visible spectrum. The most dominant peak with the widest range is concentrated in the interval from approximately 490 nm to 600 nm, with its peak localized in the 530 nm to 570 nm range. This region of the spectrum corresponds to the green to blue part of visible light. In addition to these main components, minor peaks in the ultraviolet (below 400 nm)



**Figure 5.** PL-3 polypropylene fibre knitted fabric

and infrared (above 700 nm) regions are detectable, including minor emissions around 405 nm, 580 nm, 770 nm and 800 nm. Overall, the graph confirms that the light source in question emits radiation primarily in the visible spectrum, with a dominant green component and a significant presence in the blue region.

The key to this innovation lies in the ability of the above braided structure to function as a

highly active photocatalyst. Upon absorption of photons of the corresponding wavelengths, a complex photocatalytic process is initiated on the surface of the braid. This process efficiently generates highly reactive oxygen species (ROS), which are known for their significant oxidative capacity that induces the lysis and subsequent destruction of pathogens, including COVID-19, present in the surrounding air environment. Unlike many conventional photocatalysts that require energy-intensive UV radiation, our photocatalyst concept is active under standard room illumination. This feature significantly increases its practicality, energy efficiency and overall safety in daily operation.

The antimicrobial knitted core, made up of polypropylene fibers, has been precisely designed to maximize the surface area for interaction with pathogens and to optimize the transport of photogenerated charge carriers (electrons and holes). This effectively minimizes their recombination and increases the overall quantum efficiency of the photocatalytic process. The synergistic effect of the combination of the unique braid structure

**Table 1.** Knitted fabrics tested

Designation	Type of fibre (fineness/number of fibrils)	Unit fineness (dTex/filament)	Colour	Knitting tension (cN)	Fabric density (g/m <sup>2</sup> )
PL-1	110/33 × 1	3.33	Black and blue	3.5	84.6
PL-2	125/50 × 2	2.50	black	4.0	190.1
PL-3	84/50 × 2	1.68	maroon	3.6	230.7
PL-4	56/33 × 2	1.67	Dark blue	3.5	95.0
PL-5	70/50 × 1	1.40	White	3.5	106.9
PL-6	50/50 × 2	1.00	light purple	3.5	82.1

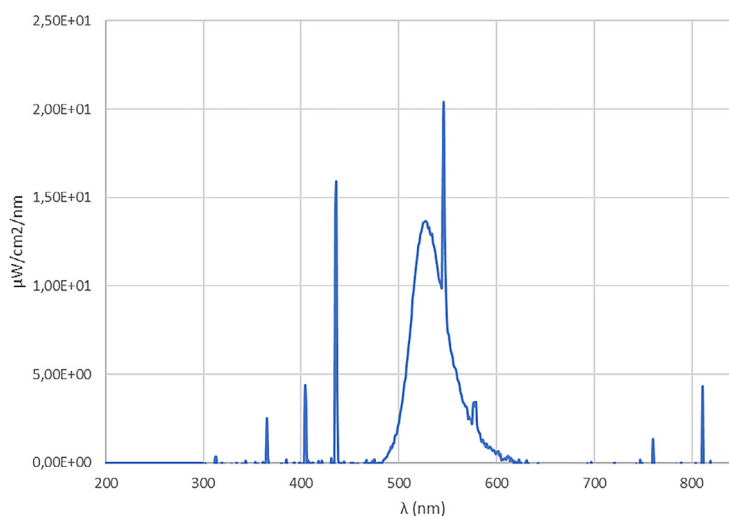


**Figure 6.** Active radiation spectrum of PL-3 knitted fabric

and photocatalytic functionality ensures not only extremely efficient but also long-lasting elimination of a wide range of microorganisms, including the viral respiratory disease COVID-19. An important benefit is also its ability to act not only on organic but also on inorganic compounds.

This research opens promising avenues for the development of a new generation of smart materials and integrated devices capable of providing continuous, passive decontamination of indoor air. Ultimately, this will contribute significantly to improving the quality of the indoor environment and enhancing public health protection.

## DETERMINATION OF AIR SATURATION WITH TOLUENE

### Antoine equation and description of saturation vapour pressure

The Clausius-Clapeyron equation is often used in physical chemistry and engineering to characterise saturation vapour pressure in relation to temperature. Its differential form leads to an integral expression Equation 1:

$$\ln \frac{p_2}{p_1} = \frac{\Delta_{vap}H}{R} \left( \frac{1}{T_1} - \frac{1}{T_2} \right) \quad (1)$$

where:  $p_1, p_2$  – saturation vapour pressures at the respective temperatures,  $T_1, T_2$  – temperature,  $\Delta_{vap}H$  – evaporative enthalpy,  $R$  – molar gas constant.

Theoretically, if the values of saturation vapor pressure at specific temperature and evaporative enthalpy were available for a given substance, this equation would allow the prediction of the functional dependence  $p = f(T)$ . However, a key limitation of this relationship is the assumption that the evaporative enthalpy ( $\Delta_{vap}H$ ) remains constant over the entire temperature range. In realistic conditions, this condition is not met, but it is necessary for the successful integration of the differential equation from which the Clausius-Clapeyron equation is derived. Practice shows that  $\Delta_{vap}H$  varies with temperature, which for some substances causes the Clausius-Clapeyron equation to be insufficiently accurate in its description. [53, 54]

An alternative approach with a similar mathematical structure is represented by the Antoine Equation 2, classified as an empirical relationship:

$$\log p = A - \frac{B}{C + T} \quad (2)$$

where:  $p$  – vapor pressure,  $T$  – temperature,  $A, B, C$  – empirical constants.

Empirical constants  $A, B, C$ , which are determined for each particular substance on the basis of experimental data. The constant  $A$  in this model symbolizes the pressure at the reference temperature, analogous to the integration constant from the boundary conditions in the Clausius-Clapeyron equation. Parameters  $B$  and  $C$  together characterize the behavior of the evaporative enthalpy. Specifically, parameter  $B$  can be interpreted as the evaporative enthalpy under reference conditions, while the constant  $C$  governs the temperature dependence of the evaporative enthalpy, allowing a better approximation of the actual behavior of the substance. Although three parameters are used, similarly to the Clausius-Clapeyron equation (if  $\Delta_{vap}H$  is assumed constant), the Antoine equation allows a more accurate description of the real dependencies. To achieve even higher accuracy, additional powers of temperature in the denominator and their associated parameters could be introduced. [53, 54] In the following Table 2 and Figure 7, the logarithmized values of Antoine's equation for calculating the density of toluene in air as a function of temperature are described and illustrated.

To calculate the ideal amount of toluene at saturated state, we used Antoine's equation at an outside temperature of 20 degrees Celsius and a pressure of 1.01 bar. Based on this, we calculated the ideal density of toluene in air Table 3, Table 4 in units of ppm, which will be compared when measuring the efficiency of the photocatalytic core formed from polypropylene knitted fabric.

### Experimental methodology

The experimental evaluation of the photocatalytic antimicrobial core's performance followed a rigorous methodology designed to ensure precision, reproducibility, and comprehensive data collection.

For the preparation and integration of the photocatalytic core, the specially developed polypropylene knitted fabric (PL-3), which serves as the carrier for the photocatalyst, was meticulously prepared and carefully integrated into the antimicrobial core of the test stand (as

**Table 2.** Logarithmized values of Antoine's equation for calculating the density of toluene in air as a function of temperature

Temperature	Parameter	Antoine's equation				
°C	K	A	B	C	$\log(P^*/\text{bar})$	$(P^*/\text{bar})$
0	273	4.23679	1426.448	-45,957	-2.0459318	0.009000
1	274	4.23679	1426.448	-45,957	-2.0183812	0.009590
2	275	4.23679	1426.448	-45,957	-1.9910711	0.010210
3	276	4.23679	1426.448	-45,957	-1.9639985	0.010860
4	277	4.23679	1426.448	-45,957	-1.9371603	0.011560
5	278	4.23679	1426.448	-45,957	-1.9105534	0.012290
6	279	4.23679	1426.448	-45,957	-1.8841748	0.013060
7	280	4.23679	1426.448	-45,957	-1.8580216	0.013870
8	281	4.23679	1426.448	-45,957	-1.832091	0.014720
9	282	4.23679	1426.448	-45,957	-1.8063801	0.015620
10	283	4.23679	1426.448	-45,957	-1.7808861	0.016560
11	284	4.23679	1426.448	-45,957	-1.7556063	0.017550
12	285	4.23679	1426.448	-45,957	-1.7305381	0.018600
13	286	4.23679	1426.448	-45,957	-1.7056786	0.019690
14	287	4.23679	1426.448	-45,957	-1.6810255	0.020840
15	288	4.23679	1426.448	-45,957	-1.6565761	0.022050
16	289	4.23679	1426.448	-45,957	-1.6323278	0.023320
17	290	4.23679	1426.448	-45,957	-1.6082783	0.024640
18	291	4.23679	1426.448	-45,957	-1.5844251	0.026040
19	292	4.23679	1426.448	-45,957	-1.5607657	0.027490
20	293	4.23679	1426.448	-45,957	-1.5372979	0.029020
21	294	4.23679	1426.448	-45,957	-1.5140193	0.030620
22	295	4.23679	1426.448	-45,957	-1.4909277	0.032290
23	296	4.23679	1426.448	-45,957	-1.4680208	0.034040
24	297	4.23679	1426.448	-45,957	-1.4452963	0.035870
25	298	4.23679	1426.448	-45,957	-1.4227522	0.037780

illustrated in Figure 4). Proper alignment and secure placement were crucial to maximize the surface area exposed to the airflow and the controlled light source.

Regarding system calibration and baseline establishment, prior to each experimental run, the mass spectrometer (Figure 1) underwent a thorough calibration process to ensure the accurate quantification of toluene concentrations. This calibration is essential for obtaining reliable and comparable results. A stable baseline concentration of toluene ( $C_{in}$ ) was established within the test stand. This was achieved by precisely controlling the evaporation rate of liquid toluene using the thermoregulation system of the Test Substance Generator. This initial concentration, theoretically determined using Antoine's equation (as detailed in Tables 2–4), was

consistently maintained before any photocatalytic activity was initiated.

Under controlled experimental conditions, measurements were systematically performed under tightly controlled environmental parameters to isolate the effect of illumination intensity on photocatalytic efficiency. A constant airflow rate of 10 liters per second (equivalent to 36 m<sup>3</sup> per hour) was maintained throughout all experiments. This specific flow rate was chosen to simulate the average volumetric air exchange typically found in standard indoor environments where such air purification devices would be deployed. The air temperature within the test environment was precisely maintained at 20 °C, and the relative humidity at 55%. These conditions were kept constant across all experimental runs to eliminate their variability as a factor influencing photocatalytic degradation. For illumination



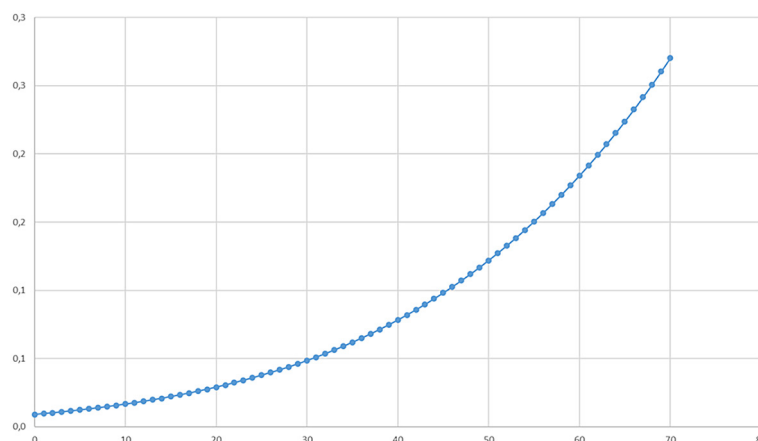


**Figure 7.** Logarithmized values of Antoine's equation for calculating the density of toluene in air as a function of temperature

**Table 3.** Logarithmized values of Antoine's equation for calculating the density of toluene in air as a function of temperature

Air	Parameter		M (toluene)	92,14	g/mol
$x(N_2)$	0.78084	(% mol)	$M(N_2)$	28.01	g/mol
$x(O_2)$	0.20946	(% mol)	$M(O_2)$	32.00	g/mol
$x(H_2O)$	0.00970	(% mol)	$M(H_2O)$	18.02	g/mol
Air pressure	1.01	bar			
Temperature	20	°C			

**Table 4.** Theoretical density of toluene after saturation

Air + toluene				
Saturated vapour pressure of toluene	0.029020	bar	$x(N_2)$	0.758203
Mole fraction of toluene vapour	0.028991		$x(O_2)$	0.203388
ppm (mol, toluene)	28991.01		$x(H_2O)$	0.009419
Mass fraction of toluene vapour	0.087333			
M of air + toluene mixture	30.59000	g/mol		

Intensities, the primary variable investigated was the illumination intensity supplied to the photocatalytic core. Experiments were conducted at 25%, 50%, 75%, and 100% of the maximum light source output. The light source was specifically configured to emit radiation primarily in the visible spectrum (mean wavelength of 500 nm within the 400–570 nm range), which corresponds to the activation spectrum of the PL-3 knitted fabric (Figure 5).

For data acquisition and efficacy measurement, the mass spectrometer, with its specialized probe, was used to quantitatively measure the concentration of toluene at two distinct points: before the air entered the antimicrobial core ( $C_{in}$ ) and after it exited the core ( $C_{out}$ ).

Measurements were captured at short, predefined time intervals, enabling real-time monitoring of the degradation dynamics and providing immediate insights into the photocatalytic process. The collected data were recorded electronically and presented graphically (Figure 9, Figure 10, Figure 11, Figure 12). The percentage decrease in toluene concentration was calculated for each measurement to determine the photocatalytic efficiency as shown in Equation 3:

$$Efficiency (\%) = \frac{(C_{in} - C_{out})}{C_{in}} \times 100 \quad (3)$$

where: *Efficiency (%)* – percentage decrease in toluene concentration, representing the

photocatalytic efficiency,  $C_{in}$  – input toluene concentration (measured before entering the antimicrobial core),  $C_{out}$  – output toluene concentration (measured after exiting the antimicrobial core).

This direct comparative method allowed for clear assessment of the photocatalyst's performance under varying illumination conditions.

Finally, for interpretation and hypothesis validation, the underlying hypothesis for this research posits that a significant degradation of toluene (specifically, at least 50% degradation) indicates substantial damage to most organic matter. Furthermore, achieving a 75% or higher reduction in toluene levels is considered a strong indicator for effective elimination of a wide range of airborne pathogens, including viral agents like COVID-19. The experimental results were analyzed in light of this hypothesis to confirm the broad-spectrum potential of the tested material.

## Experimental results

After careful preparation and application of the polypropylene knitted fabric to the device (Figure 8), which serves as a carrier for the photocatalyst, the test bench was ready to measure

the performance of the antimicrobial filter. The efficiency is measured using a mass spectrometer, which is applied with a special probe from above into the test environment (Figure 8). This instrument allows the concentration of the test substance to be accurately quantified before entering and after leaving the antimicrobial core. Measurements are taken at short time intervals, which is critical for immediate evaluation of the dynamics of the degradation process.

The measurements were performed on the test bench at illumination intensities of 25% (Table 5), 50% (Table 6), 75% (Table 7) and 100% (Table 8) at a constant airflow rate of 10 liters per second, which is 36 m<sup>3</sup> per hour, and this is the average volumetric size of the room where it is to be deployed.

The measurement of toluene degradation at 25% illumination intensity is shown graphically in the following Figure 9.

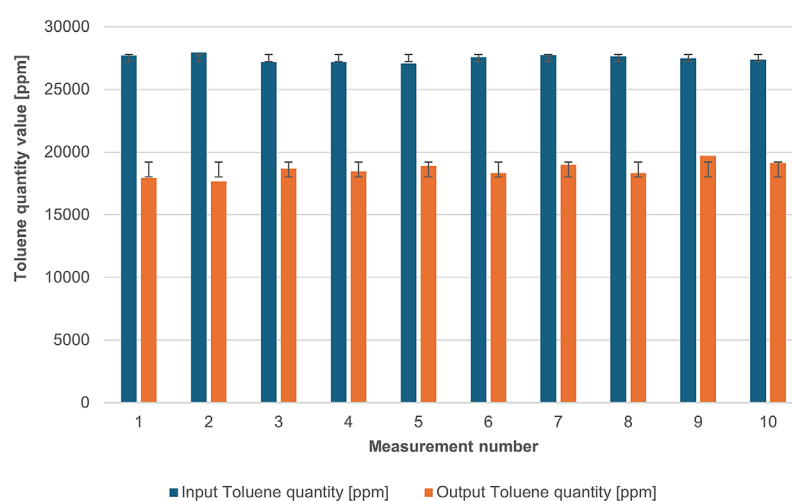
The air temperature was 20 °C and the humidity was 55%. We hypothesized that the photocatalytic reaction results in the oxidation of toluene, and in the case of at least 50% toluene degradation, most organic matter will be damaged. As can be seen from the following measurements (Table 5) 25% illumination intensity is insufficient for the expected photocatalytic efficiency, 50% illumination intensity (Table 6)



**Figure 8.** Measurement of test bench performance using sensors and probes

**Table 5.** Measurement of toluene degradation at 25% illumination intensity

Measurement number	Illumination intensity	Air temperature [°C]	Input value of Toluene quantity [ppm]	Toluene output value [ppm]	Percentage decrease
1	25%	20	27714	17946	35.25%
2	25%	20	27942	17667	36.77%
3	25%	20	27202	18668	31.37%
4	25%	20	27205	18435	32.23%
5	25%	20	27078	18892	30.23%
6	25%	20	27585	18319	33.59%
7	25%	20	27729	18989	31.52%
8	25%	20	27621	18313	33.70%
9	25%	20	27492	19709	28.31%
10	25%	20	27387	19121	30.18%


**Figure 9.** Measurement of toluene degradation at 25% illumination intensity

is at the limit of the desired photocatalytic efficiency. For a given photocatalytic filter size, at least 75% illumination intensity satisfies the conditions (Table 7, Table 8). The measurement of toluene degradation at 50% illumination intensity

is shown graphically in Figure 10. The measurement of toluene degradation at 75% illumination intensity is shown graphically in Figure 11.

As we predicted at 100% illumination intensity, there should be at least a 75% decrease in the

**Table 6.** Measurement of toluene degradation at 50% illumination intensity

Measurement number	Intensity of enlightenment	Air temperature [°C]	Input Toluene quantity [ppm]	Toluene quantity output [ppm]	Percentage decrease
1	50%	20	27802	12035	56.71%
2	50%	20	27765	11358	59.09%
3	50%	20	27747	11507	58.52%
4	50%	20	27236	11523	57.69%
5	50%	20	27193	12222	55.05%
6	50%	20	27619	12582	54.44%
7	50%	20	27925	11762	57.88%
8	50%	20	27652	12172	55.98%
9	50%	20	27589	11834	57.10%
10	50%	20	27267	11984	56.04%

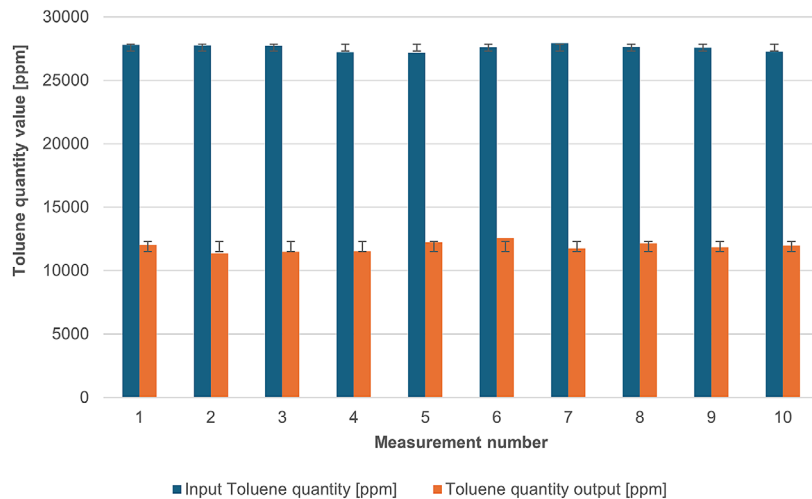


**Figure 10.** Measurement of toluene degradation at 50% illumination intensity

**Table 7.** Measurement of toluene degradation at 75% illumination intensity

Measurement number	Intensity of enlightenment	Air temperature [°C]	Input Toluene quantity [ppm]	Toluene quantity output [ppm]	Percentage decrease
1	75%	20	27286	8724	68.02%
2	75%	20	27987	8778	68.63%
3	75%	20	27000	8640	68.00%
4	75%	20	27068	8694	67.88%
5	75%	20	27929	8627	69.11%
6	75%	20	27155	8819	67.52%
7	75%	20	27212	8960	67.07%
8	75%	20	27893	8790	68.48%
9	75%	20	27060	8543	68.42%
10	75%	20	27321	8564	68.65%

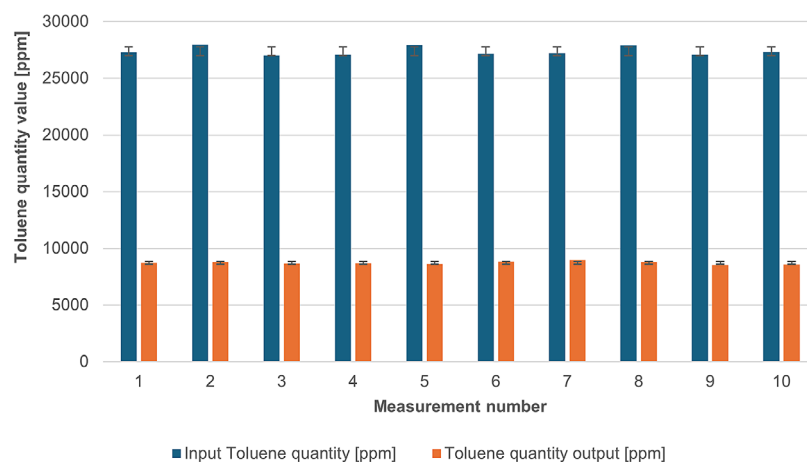


**Figure 11.** Measurement of toluene degradation at 75% illumination intensity

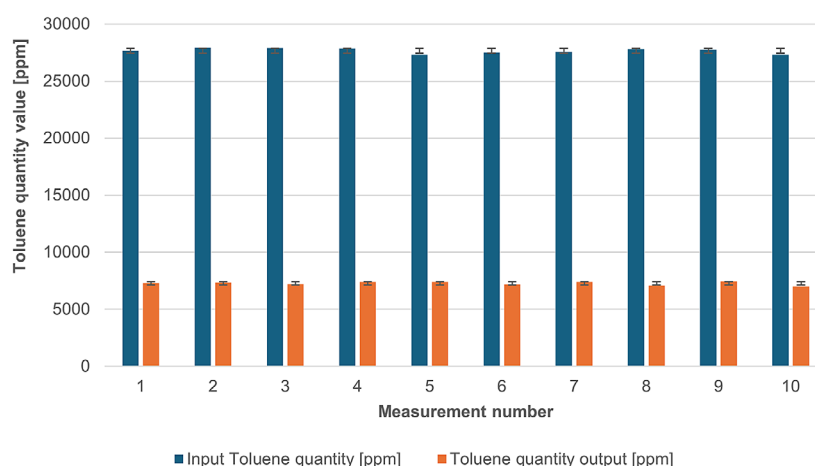
toluene level, which will ensure the elimination of pathogens. In the case of an increase in efficiency, it would be necessary to increase the filter area and increase the illumination intensity.

For the measurements, we used the mean value of the colour spectrum of 500 nm from the range of 400–570 nm required by the manufacturer of the photocatalytic substance present in the braid.



**Table 8.** Measurement of toluene degradation at 100% illumination intensity

Measurement number	Intensity of enlightenment	Air temperature [°C]	Input Toluene quantity [ppm]	Toluene quantity output [ppm]	Percentage decrease
1	100%	20	27668	7304	73.60%
2	100%	20	27941	7343	73.72%
3	100%	20	27882	7214	74.13%
4	100%	20	27855	7423	73.35%
5	100%	20	27331	7410	72.89%
6	100%	20	27498	7201	73.81%
7	100%	20	27556	7422	73.07%
8	100%	20	27812	7071	74.58%
9	100%	20	27758	7456	73.14%
10	100%	20	27327	7010	74.35%

**Figure 12.** Measurement of toluene degradation at 100% illumination intensity

Changing the wavelength to the extremes of the range (400 and 570 nm) did not produce a measurable improvement in the efficiency of the photocatalytic filter. The measurement of toluene degradation at 100% illumination intensity is shown graphically in the following Figure 12.

During experimental testing, the temperature can be flexibly controlled to optimize the rate of toluene evaporation. At the same time, dust and overall air pollution levels are monitored and modified, contributing to the versatility of the device. Configuration of several operating parameters such as air flow volume per minute, temperature, humidity and dust level is provided by the aforementioned integrated sensors and control system.

## CONCLUSIONS

The research presented in this paper focused on the development and characterization of a

photocatalytic efficacy test-bed that was designed as a direct response to the urgent need for efficient, inexpensive, and highly effective air decontamination and pathogen elimination, particularly in the context of global pandemic challenges. This innovative bench is used to accurately evaluate the performance of a new type of device that incorporates a photocatalytic antimicrobial core based on a polypropylene knitted fabric that is active under normal illumination. The testing methodology uses toluene as a model volatile organic compound, the concentration of which is monitored by a mass spectrometer, allowing immediate evaluation of the degradation dynamics, thus ensuring efficient verification of its functionality.

The measurements performed confirmed the ability of the photocatalytic antimicrobial core to degrade toluene at different illumination intensities. At 25% illumination intensity, an average toluene degradation of approximately 32.2%

was recorded, which was evaluated as insufficient for the expected photocatalytic efficiency. Increasing the intensity to 50% resulted in an average degradation of about 56.8%, which was at the limit of the desired photocatalytic efficiency. At 75% illumination intensity, an average degradation of about 68.3% was achieved. Finally, at 100% illumination intensity, the tests showed an average decrease in toluene concentration of around 73.6%. Based on the hypothesis that at least 50% degradation of toluene leads to the deterioration of most organic matter, and with the assumption of a 75% decrease in toluene levels to ensure pathogen elimination, these results confirm the considerable potential of the tested material. To achieve higher efficiency, the filter area would need to be increased and the illumination intensity increased.

The developed test bench, whose design is protected by a utility model, represents a robust and adaptable solution for the comprehensive evaluation of photocatalytic materials. Its main advantages are the ability to test a wide range of substances, including both organic and inorganic compounds, the immediate evaluation of results thanks to the mass spectrometer, and the flexible configuration of operating parameters such as temperature, humidity and dust level. This comprehensive methodology not only quantifies the performance of the photocatalyst in an exact manner, but also allows a deeper understanding of its mechanisms of operation and confirms its potential for large-scale practical applications in the field of continuous and passive indoor air decontamination. Ultimately, this research contributes significantly to improving the quality of the indoor environment and enhancing public health protection.

### Acknowledgements

This article is based on the ITMS 2014+ project 313011AVF5 INTELTEX – Centre for the Development of Textile Intelligence and Antimicrobial Technologies, project KEGA 040TUKE-4/2025 – Implementation of Additive Technologies in Selected Profile Subjects in the field of Mechanical Engineering to Increase the Creativity of Students Using the Connection with a foreign University Environment, and project APVV-23-0364 – Identification and Quantification of Key Parameters of Core Drilling of Rocks by New Diagnostic Methods.

### REFERENCES

1. Murray PR, Rosenthal KS, Pfaller MA. Medical Microbiology. 9th ed. Philadelphia: Elsevier; 2021.
2. Snyder L, Peters JE. Molecular Genetics of Bacteria. 5th ed. Washington, D.C.: ASM Press; 2020.
3. Prescott LM, Willey JM, Sherwood LM, Woolverton CJ. Prescott's Microbiology. 12th ed. New York: McGraw-Hill Education; 2023.
4. World Health Organization. Antimicrobial Resistance: Global Report on Surveillance 2021. Geneva: World Health Organization; 2021.
5. World Health Organization. COVID-19 and the impact on antimicrobial resistance: One Health approach. Geneva: World Health Organization; 2022.
6. Manyi-Loh CE, et al. Antibiotic resistance in the One Health era: The global perspective. Mol Biol Rep. 2023;50(1):2507–25. <https://doi.org/10.1007/s11033-022-08034-w>
7. Madigan MT, Martinko JM, Bender KS. Brock Biology of Microorganisms. 15th ed. Boston: Pearson; 2018.
8. Flint SJ, Racaniello VR, Rall GF. Principles of Virology. 5th ed. Washington, DC: ASM Press; 2020.
9. Mohanty SK, Das K, Panda AP. Global Viral Pandemics: A Comprehensive Overview of Etiology, Epidemiology, and Impact. J Infect Dis Epidemiol [Internet]. 2023;9(2):1-10. Available from: <https://www.longdom.org/open-access/global-viral-pandemics-a-comprehensive-overview-of-etiology-epidemiology-and-impact-JIDE-23-455.pdf> [Accessed 2025 Jun 22].
10. Peiris JSM, Horby P, Leung G. Viral Pandemics: A Perpetual Threat and the Need for Preparedness. Lancet Glob Health. 2023;11(10): e1537–48. [https://doi.org/10.1016/S2214-109X\(23\)00293-8](https://doi.org/10.1016/S2214-109X(23)00293-8)
11. Nyako M, et al. Global epidemic burden and case fatality rates of major viral hemorrhagic fevers: a systematic review and meta-analysis. J Infect Dis Epidemiol [Internet]. 2023;9(4):1–12. Available from: <https://www.longdom.org/open-access/global-epidemic-burden-and-case-fatality-rates-of-major-viral-hemorrhagic-fevers-a-systematic-review-and-metaanalysis-JIDE-23-455.pdf> [Accessed 2025 Jun 22].
12. Fan Y, et al. Global health security: challenges and strategies in the post-COVID-19 era. Front Public Health. 2024; 12:1380962. <https://doi.org/10.3389/fpubh.2024.1380962>
13. Armstrong-James D, et al. Global burden of serious fungal infections. Front Microbiol. 2023; 14:1209355. <https://doi.org/10.3389/fmicb.2023.1209355>
14. Block SS, editor. Disinfection, Sterilization, and Preservation. 6th ed. Philadelphia: Lippincott Williams & Wilkins; 2020.

15. Rutala WA, Weber DJ. Disinfection, sterilization, and antisepsis: An overview. *Am J Infect Control*. 2016;44(5): e1–6. [https://doi.org/10.1016/S0196-6553\(16\)00004-8](https://doi.org/10.1016/S0196-6553(16)00004-8)
16. Ghani M, et al. Thermal inactivation of viruses: principles and applications. *Curr Opin Virol*. 2023; 60:101291. <https://doi.org/10.1016/j.coviro.2023.101291>
17. World Health Organization. UV-C radiation and COVID-19: What you need to know [Internet]. Geneva: World Health Organization; 2020. Available from: <https://www.who.int/news-room/q-a-detail/uv-c-radiation-and-covid-19-what-you-need-to-know> [Accessed 2025 Jun 22].
18. Chen J, et al. Ionization for air purification: principles, performance, and health effects. *Environ Sci Technol*. 2022;56(1):121–35. <https://doi.org/10.1021/acs.est.1c03975>
19. Wang H, et al. Effects of air ions on human health and wellbeing: a systematic review. *Environ Res*. 2023; 231:116172. <https://doi.org/10.1016/j.envres.2023.116172>
20. Ahmad MN, et al. Membrane filtration for water and wastewater treatment: principles, recent advances, and future challenges. *Membranes*. 2023;13(8):741. <https://doi.org/10.3390/membranes13080741>
21. Kowalski WJ. Ultraviolet Germicidal Irradiation Handbook: UVGI for Air and Surface Disinfection. 3rd ed. Berlin: Springer; 2023.
22. Kuzin S, et al. Ethylene oxide: environmental and health aspects. *Curr Environ Health Rep*. 2022;9(4):556–65. <https://doi.org/10.1007/s40572-022-00366-z>
23. McNamarra A, et al. Disinfectants: Mechanism of action and application. *Curr Protoc Microbiol*. 2022;65(1): e138. <https://doi.org/10.1002/cpmc.138>
24. United States Environmental Protection Agency (EPA). What is a HEPA filter? [Internet]. Washington, D.C.: U.S. EPA; 2024. Available from: <https://www.epa.gov/indoor-air-quality-iaq/what-hepa-filter> [Accessed 2025 Jun 22].
25. Sharma A, et al. Air purifiers in the fight against COVID-19 and other airborne pathogens. *Appl Sci*. 2023;13(1):288. <https://doi.org/10.3390/app13010288>
26. Saraf M, et al. Air purifiers and human health: a review of efficacy and health outcomes. *Environ Sci Pollut Res*. 2023;30(1):1–15. <https://doi.org/10.1007/s11356-022-24317-5>
27. Khan S, et al. Ozone: An effective oxidant for disinfection of water and wastewater. *J Environ Chem Eng*. 2022;10(6):108711. <https://doi.org/10.1016/j.jece.2022.108711>
28. Zhao Q, et al. Ozone disinfection for inactivating viruses: current understanding and future directions. *Environ Sci Technol Lett*. 2024;11(2):109–17. <https://doi.org/10.1021/acs.estlett.3c00845>
29. U.S. Environmental Protection Agency (EPA). Ozone Generators that are Sold as Air Cleaners: An Assessment of Health Effects and Effectiveness [Internet]. Washington, D.C.: U.S. EPA; 2022. Available from: <https://www.epa.gov/indoor-air-quality-iaq/ozone-generators-are-sold-air-cleaners-assessment-health-effects-and-effectiveness> [Accessed 2025 Jun 22].
30. Rajasekaran A, et al. Recent advances in hybrid technologies for disinfection of water and wastewater. *J Clean Prod*. 2023; 426:138981. <https://doi.org/10.1016/j.jclepro.2023.138981>
31. Ma C, et al. Integrated air purification technologies for indoor environments: A review. *Build Environ*. 2024; 250:111166. <https://doi.org/10.1016/j.buildenv.2023.111166>
32. Wang C, et al. Review on indoor air purifiers and their effects on human health. *Build Environ*. 2023; 240:110488. <https://doi.org/10.1016/j.buildenv.2023.110488>
33. Jang K, et al. Performance evaluation of combination air purifiers. *Indoor Air*. 2024;34(1): e12933. <https://doi.org/10.1111/ina.12933>
34. Ohtani B. What Is photocatalysis? – definition, mechanistic aspects, and its history. *J Photochem Photobiol C Photochem Rev*. 2010;11(3–4):157–78. <https://doi.org/10.1016/j.jphotochemrev.2010.12.001>
35. Schuhmann W, et al. A critical review of photocatalysis: definitions, mechanisms, and common pitfalls. *J Catal*. 2023; 423:115049. <https://doi.org/10.1016/j.jcat.2023.115049>
36. Wang F, et al. Recent advances in photocatalysis for sustainable energy and environmental applications. *Green Energy Environ*. 2024;9(2):227–51. <https://doi.org/10.1016/j.gee.2023.06.002>
37. Li W, et al. Recent advances in metal oxides as photocatalysts: a review. *Mater Today Energy*. 2023;35:101373. <https://doi.org/10.1016/j.mtener.2023.101373>
38. Zhang X, et al. Carbon-based materials for photocatalysis: A review. *Carbon*. 2023; 209:118025. <https://doi.org/10.1016/j.carbon.2023.118025>
39. Qiao L, et al. Recent advances in 2D materials for photocatalysis. *Mater Today Nano*. 2023;24:100378. <https://doi.org/10.1016/j.mtnano.2023.100378>
40. Das S, et al. Quantum dots in photocatalysis: Recent advances and challenges. *J Mater Sci*. 2023;58(1):1–28. <https://doi.org/10.1007/s10853-023-08573-0>
41. Dai W, et al. Phase engineering of photocatalysts: Strategies, challenges, and perspectives. *Energy Environ Sci*. 2024;17(3):1217–49. <https://doi.org/10.1039/D3EE03463J>
42. Anpo M, et al. Critical aspects in photocatalysis: kinetic models and the importance of initial rate

- determination. *Chem Lett.* 2024;53(2):110–8. <https://doi.org/10.1246/cl.230491>
43. ISO (International Organization for Standardization). ISO 22197: Photocatalysis – Test methods for air purification and water treatment [Internet]. Geneva: ISO; [cited 2025 Jul 8]. Available from: <https://www.iso.org/standard/76503.html>.
44. ISO (International Organization for Standardization). ISO 20814:2019 Nanotechnologies – Photocatalytic TiO<sub>2</sub> – Test method for antibacterial activity under UV irradiation [Internet]. Geneva: ISO; 2019. Available from: <https://www.iso.org/standard/74737.html>
45. Cui K, et al. A rapid, high-throughput method for evaluating photocatalytic activity on gypsum boards. *Constr Build Mater.* 2024; 412:134676. <https://doi.org/10.1016/j.conbuildmat.2023.134676>
46. Chen DD, et al. A novel turbidimetric method for evaluating the photocatalytic activity of suspended fine particles. *J Hazard Mater.* 2023;446:130704. <https://doi.org/10.1016/j.jhazmat.2022.130704>
47. Khan MNA, et al. Air pollution and its impact on human health: A review. *Environ Sci Pollut Res.* 2023;30(10):26868–80. <https://doi.org/10.1007/s11356-022-24317-5>
48. Li Y, et al. Polypropylene melt-blown nonwovens for air filtration: a review of fabrication and performance. *Polymers.* 2023;15(19):4038. <https://doi.org/10.3390/polym15194038>
49. SolidWorks. What is SolidWorks? [Internet]. [cited 2025 Jun 25]. Available from: <https://www.solidworks.com/what-is-solidworks>.
50. Úrad priemyselného vlastníctva Slovenskej republiky. Úžitkový vzor 9998 [Internet]. Banská Bystrica: Úrad priemyselného vlastníctva Slovenskej republiky; 2024. Available from: <https://wbr.indprop.gov.sk/WebRegistre/UzitkovyVzor/Detail/50049-2023?csrt=4650112789111951247>
51. Král J, Dzuro T, Novotný D, Melko J, Valo M. Základy počítačovej geometrie. Košice: Strojnícka fakulta, Technická univerzita v Košiciach; 2024.
52. V&F. V&F AirSense Mass spectrometer [Internet]. [cited 2025 Jun 28]. Available from: <https://www.vandf.com/en/products/analyzers/vf-airsense/>.
53. Pitzer KS, Scott DW. The thermodynamics and molecular structure of benzene and its methyl derivatives. *J Am Chem Soc.* 1943;65:803–29.
54. Besley LM, Bottomley GA. Vapour pressure of toluene from 273.15 to 298.15 K. *J Chem Thermodyn.* 1974;6(6):577–80. [https://doi.org/10.1016/0021-9614\(74\)90045-7](https://doi.org/10.1016/0021-9614(74)90045-7)